Chinese Journal of Aeronautics, (2016), 29(5): 1414–1424

Chinese Society of Aeronautics and Astronautics
& Beihang University

Chinese Journal of Aeronautics

cja@buaa.edu.cn
www.sciencedirect.com

Comparative investigation on high-speed grinding of TiCp/Ti–6Al–4V particulate reinforced titanium matrix composites with single-layer electroplated and brazed CBN wheels

Li Zheng, Ding Wenfeng *, Shen Long, Xi Xinxin, Fu Yucan

College of Mechanical and Electrical Engineering, Nanjing University of Aeronautics and Astronautics, Nanjing 210016, China

Received 13 October 2015; revised 23 November 2015; accepted 14 December 2015
Available online 14 January 2016

KEYWORDS

High-speed grinding;
PTMCs;
Single-layer brazed CBN wheel;
Single-layer electroplated CBN wheel;
Surface defects

Abstract In order to develop the high-efficiency and precision machining technique of TiCp/Ti–6Al–4V particulate reinforced titanium matrix composites (PTMCs), high-speed grinding experiments were conducted using the single-layer electroplated cubic boron nitride (CBN) wheel and brazed CBN wheel, respectively. The comparative grinding performance was studied in terms of grinding force, grinding temperature, grinding-induced surface features and defects. The results display that the grinding forces and grinding temperature obtained with the brazed CBN wheel are always lower than those with the electroplated CBN wheel. Though the voids and microcracks are the dominant grinding-induced surface defects, the brazed CBN wheel produces less surface defects compared to the electroplated wheel according to the statistical analysis results. The maximum materials removal rate with the brazed CBN wheel is much higher than that with the electroplated one. All above indicate that the single-layer brazed CBN super-abrasive wheel is more suitable for high-speed grinding of PTMCs than the electroplated counterpart.

1. Introduction

TiCp/Ti–6Al–4V particulate reinforced titanium matrix composites (PTMCs) have high specific strength, high wear resistance and high temperature durability, which show great application potentials as important structural materials in the aerospace and military industries.[1–3] However, similar to SiCp/Al aluminum matrix composites, it is also very difficult to machine PTMCs due to the co-existence of hard TiC reinforcements and high-strength Ti–6Al–4V matrix.[4–6] Bejjani

* Corresponding author. Tel.: +86 25 84892901.
E-mail address: dingwf2000@vip.163.com (W. Ding).
Peer review under responsibility of Editorial Committee of CJA.

http://dx.doi.org/10.1016/j.cja.2016.01.005

et al.[7] have studied the effects of cutting parameters with PCD on tool life, chip morphology and surface integrity in laser assisted turning of titanium metal matrix composite. They discovered that tool life could be enhanced for laser assisted machining of titanium metal matrix composite, however, surface roughness moderately increased by up to 15%. Aramesh et al.[8] tested the tool wear in turning titanium metal matrix composite using PCD cutting tool. Statistical model was developed to estimate the average service life of the cutting inserts during turning Ti-MMCs, and initial wear, steady wear and rapid wear regions in the tool wear curve were regarded as the different states in the statistical model. Besides the severe tool wear, poor surface quality is another machining problem in the cutting and grinding process.[9,10] For example, Blau and Joll[9] discovered that the reinforcing particles were easily fractured and pulled out in the grinding practice of titanium matrix composites with the vitrified alumina abrasive wheels. At the same time, some clusters of fragments also remained on the surface or were trapped in microcracks. Under such condition, the ground surface quality of PTMCs would be degraded even though the maximum materials removal rate applied is only 0.5 $mm^3/(mm\ s)$. For the above reason, how to realize high-efficiency and precision machining of PTMCs becomes an important research topic in the present days.

Single-layer electroplated cubic boron nitride (CBN) super-abrasive wheels, owing to their good properties of high hardness, high thermal conductivity, high wear resistance and high chemical inertness, have been applied to grind difficult-to-cut materials. Marschalkowski et al.[11] carried out the grinding of 102Cr6 hardened bearing steel (63 HRC) using electroplated CBN wheels. The advantages in increasing the grinding efficiency and improving the probability of wheel life were verified. Aspinwall et al.[12] investigated the tool wear and surface integrity in grinding Udimet 720 nickel-based superalloy. It was found that the tool life of the electroplated CBN wheel was longer than that of electroplated diamond super-abrasive wheel; furthermore, surface burnout didn't happen under the test conditions when using the electroplated CBN wheels.

On the other hand, in recent years, more and more attention has been paid to the single-layer brazed CBN wheels because the precision brazing process could build a strong chemical bridge between CBN grains and wheel substrate with the help of Ag–Cu–Ti active filler alloy as the bonding material. As a consequence, the single-layer brazed CBN wheels could provide stronger bonding to grains, higher grain protrusion and more favorable grain distribution than the electroplated CBN wheels, which is much beneficial to further improve the grinding performance of the CBN super-abrasive wheels. Teicher and Ghosh conducted grinding of Ti–6Al–4V titanium alloy using the single-layer brazed CBN wheels.[13] Low grinding temperature and good surface quality were obtained. Ding and Xu carried out the profile creep-feed grinding of K417 cast nickel-based superalloy with the brazed CBN wheel.[14] Low grinding temperature at about 100 °C was obtained. Furthermore, all the required dimensional accuracy, surface roughness and comprehensive residual stresses of the straight groove components were reached under the optimum grinding parameters as follows: the wheel speed of 22.5 m/s, the workpiece speed of 0.10 m/min, and the depth of cut of 0.20 mm.

High-speed grinding with CBN super-abrasive wheels has been regarded as a desirable method to improve the machined surface quality in high-efficiency grinding. The reason is mainly attributed to the decreasing undeformed chip thickness and the possible ductile removal mode of the brittle materials during the high-speed grinding process.[15–18] In other words, the difficulty in machining difficult-to-cut materials is perhaps weakened to a certain extent in high-speed grinding. For example, Tian et al. found that the grinding temperature could be controlled effectively in high-speed grinding of Ti–6Al–4V titanium alloy; accordingly, the grinding-induced surface quality was improved.[19]

In order to provide an experimental and theoretical basis for high-efficiency and precision machining of PTMCs, high-speed grinding experiments are carried out with the single-layer electroplated CBN wheel and brazed CBN counterpart, respectively, in the current investigation. The comparative grinding performance of PTMCs with the two types of single-layer CBN wheels is analyzed comprehensively in terms of grinding force, grinding temperature and grinding-induced surface features and defects.

2. Experimental details

The PTMCs contain Ti–6Al–4V metal matrix and 10 vol% TiC reinforcing particles, which are produced by the state key laboratory of metal matrix composites of China. The TiC reinforcing particles with a size of 1.2–8.4 μm are synthesized by means of powder metallurgy technique in the fabrication process of PTMCs. The average quantity of TiC particles is about $1500/mm^2$ (Fig. 1). Meanwhile, a small quantity of TiB whiskers is also contained in PTMCs. The composition and mechanical properties are listed in Table 1.

Grinding experiments are performed on a high-speed surface grinder, BLOHM PROFIMAT MT-408. The maximum rotational speed is 8000 r/min and the output power is 45 kW. Fig. 2 schematically demonstrates the experimental

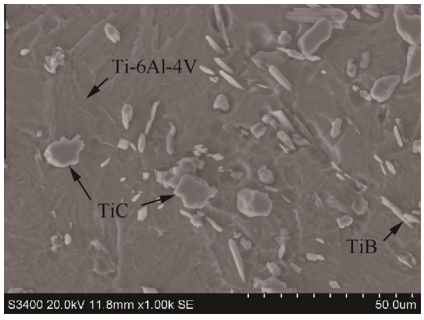

Fig. 1 Microstructure of TiCp/Ti–6Al–4V composites.

Table 1 Composition and mechanical properties of PTMCs.

Content	Value
Matrix	Ti–6Al–4V
Reinforcements	10 vol.% TiC particles
Tensile strength	1102 MPa
Yield strength	972 MPa
Elongation rate	0.55%
Elasticity modulus	133 GPa
Poisson's ratio	0.34

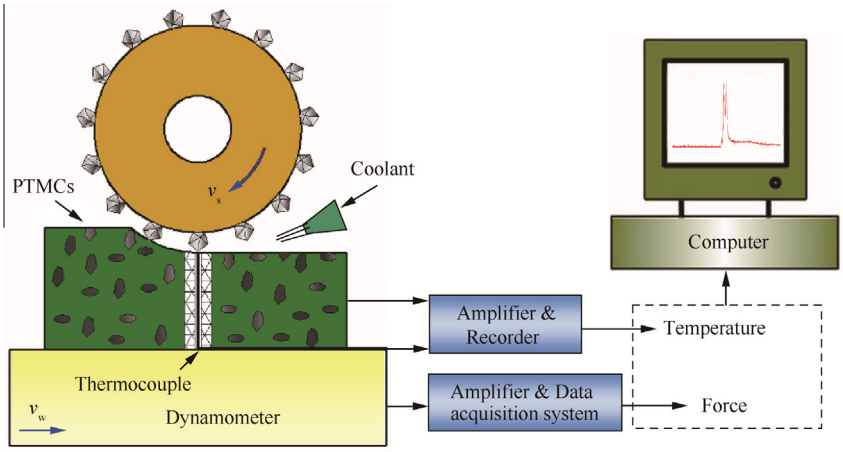

Fig. 2 Schematics of the grinding experimental set-up with single-layer CBN wheel.

set-up. Up-grinding mode is applied. Fig. 3(a) displays the whole morphology of single-layer CBN wheels. The outer diameter of the wheel is 400 mm, and the grain size is 80/100 mesh. In particular, the grain particles are distributed randomly on the working surface of the electroplated CBN wheel (Fig. 3(b)), while they are distributed linearly with a row interval of 1.2 mm on the working surface of the brazed wheel (Fig. 3(c)). The electroplated CBN wheel is fabricated by Suzhou Wente Super-abrasive Tools Co. Ltd., China. The brazed CBN wheel is fabricated by the authors. The fabrication technology of the single-layer brazed CBN wheels has been introduced in the previous publication.[20] The bonding material of the brazed CBN wheel is $(Ag_{72}Cu_{28})_{95}Ti_5$ (wt%) alloy, and the brazing temperature is 920 °C.

The details of the current grinding conditions are listed in Table 2. The wheel speed v_s was fixed at 120 m/s, which was a broadly accepted wheel speed for high-speed grinding of difficult-to-cut materials in the present days. The workpiece infeed speeds v_w was varied among 3, 6, 9, 12 m/min, and the depth of cut a_p was among 0.005, 0.010, 0.015, 0.020 mm. Grinding forces signals were measured using the piezoelectric dynamometer Kistler 9272. The grinding temperature signals were captured by means of the semi-artificial thermocouple technique.[21] Before grinding, the PTMCs workpiece samples were cut equally to two blocks with the size of 15 mm (length) × 5 mm (width) × 25 mm (height). A constantan foil of 0.020 mm thickness was sandwiched between couples of workpiece and was insulated by two mica sheets. A hot junction for a constantan-workpiece semi-artificial thermocouple was made in the grinding process. The thermal electromotive signal was therefore formed and the grinding temperature could be measured using a Labview data acquisition card connected to a computer, as displayed in Fig. 2.

Table 2 Grinding experimental conditions.

Contents	Values
Machine tool	Surface grinding machine modeled BLOHM PROFIMAT MT-408
Grinding mode	Up-grinding
Wheel speed v_s	120 m/s
Workpiece infeed speed v_w	3–12 m/min
Depth of cut a_p	0.005–0.020 mm
Grinding width b	5 mm
Cooling fluid	Emulsified liquid; 5% dilution; 90 L/min; Pressure at 15 MPa

After grinding, the PTMCs surface was observed using Hirox KH-7700 optical microscopy and Quanta-200 scanning electron microscopy (SEM). The corresponding defects were quantitatively statistically analyzed.

3. Results and discussion

3.1. Comparison of grinding force in high-speed grinding

Grinding force is an important index to evaluate the grinding performance.[22,23] Comparative analysis on the grinding forces of the electroplated CBN wheel and brazed CBN wheel was carried out at the identical high-speed grinding parameters.

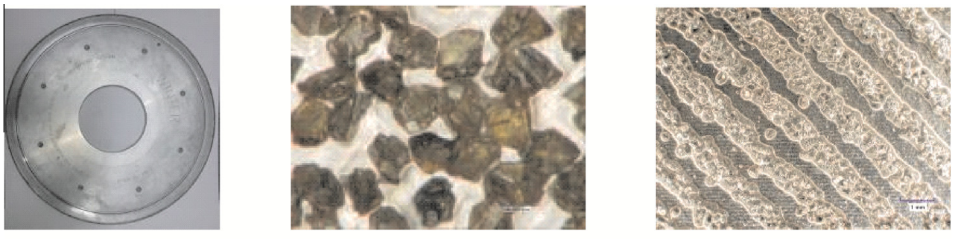

(a) Whole profile (b) Electroplated CBN wheel (c) Brazed CBN wheel

Fig. 3 Single-layer CBN wheels.

Fig. 4 shows the measured signal of the normal force F_n and tangential force F_t, with different single-layer CBN wheels at the identical grinding parameters, i.e., the wheel speed of 120 m/s, the workpiece infeed speed of 6 m/min and depth of cut of 0.010 mm during high-speed grinding of PTMCs. Fig. 5 displays the effects of the grinding parameters on the grinding forces. Seen from Fig. 5(a), an increase in workpiece infeed speed leads to increasing of both the normal and tangential grinding forces. When the depth of cut is kept at 0.010 mm, and the workpiece infeed speed increases from 3 m/min to 12 m/min, the normal force F_n increases from 26.2 N to 43.8 N (by 67%) with the electroplated CBN wheel and from 19.7 N to 37.4 N (by 90%) with the brazed counterpart, respectively. Meanwhile, the tangential force F_t rises from 6.5 N to 9.8 N (by 51%) with the electroplated CBN wheel and from 4.5 N to 7.8 N (by 73%) with the brazed one, respectively.

When the depth of cut increases from 0.005 mm to 0.020 mm and the workpiece infeed speed is fixed at 6 m/min, the normal force rises rapidly from 26.5 N to 48.7 N (by 84%) and the tangential force also increases from 6.0 N to 10.5 N (by 75%) with the electroplated CBN wheel (Fig. 5 (b)). For the brazed CBN wheel, the recorded normal force rises from 20.0 N to 43.0 N (by 115%), and the tangential force increases approximately from 4.5 N to 7.6 N (by 67%). In general, lower grinding force obtained with the brazed CBN wheel is mainly attributed to the higher grain protrusion on the tool surface, which increases the sharpness degree and enlarges the chip storage space of the CBN super-abrasive wheel during grinding.[18]

3.2. Comparison of grinding temperature in high-speed grinding

During grinding difficult-to-cut materials, a great amount of energy is converted to the grinding heat within the tool-workpiece contact zone, most of which eventually is transferred into the workpiece and causes a grinding temperature rise.[24–26] Fig. 6 displays two typical grinding temperature curves measured using the thermocouples, which correspond to different single-layer CBN wheels at the identical grinding parameters, i.e., the wheel speed of 120 m/s, the workpiece infeed speed of 6 m/min and depth of cut of 0.010 mm. Obviously, the grinding temperature (T) of 703 °C with the electroplated CBN wheel is much higher than that of 569 °C with the brazed counterpart. At this time, the burnout phenomenon could take place on the surface ground with the electroplated CBN wheel (Fig. 7(a)); on the contrary, good ground surface is produced with the brazed wheel (Fig. 7(b)).

Because the grinding temperature beneath the workpiece surface could not be measured directly by the semi-artificial thermocouple method in the current investigation, a three-dimensional (3D) finite element model (FEM) based on a moving triangular heat source was established to simulate the temperature distribution. The initial temperature considered for the workpiece is the room temperature, i.e., $T = 20$ °C. In wet grinding, the convective cooling is applied on the top surface to represent coolant application. A heat transfer coefficient of 82,000 W/m^2 is used to simulate the cooling effects of the grinding coolant fluid passing through the workpiece in a grinding pass.[27] The bottom surface of the workpiece is regarded as thermally insulated from the environment. According to Newton's cooling law, this means that there is no heat loss from the workpiece to the environment. The characteristic of the moving triangular heat source and convective cooling during grinding is illustrated in Fig. 8. The mesh method was applied to deal with the sharp temperature gradient in the workpiece top region, while keeping a reasonable element size to reduce the calculating time. Therefore, the fine elements were designed in the workpiece top region, and the coarse ones were in the bottom region of the ground workpiece. The component was meshed using 20-nodes hex elements. The heat flux applied for the finite element simulation was computed from the average values of the tangential grinding forces, which varied from 3.49×10^7 W/m^2 to 6.48×10^7 W/m^2.[28]

Fig. 9 displays the results of the simulated temperature distribution contours within the workpiece ground with the electroplated and brazed CBN wheels, respectively. The grinding parameters are as follows: the wheel speed of 120 m/s, the workpiece infeed speed of 6 m/min, and the depth of cut of 0.010 mm. As for the grinding temperature, the 3D FEM results and those measured by the semi-artificial thermocouple method show a good consistency (Fig. 6). High grinding temperature is always produced within the tool-workpiece contact zone when the thermal source moves along the workpiece surface. The heat conducted into the workpiece is transferred away to the surroundings during grinding, which results in a temperature field tail (Fig. 9).

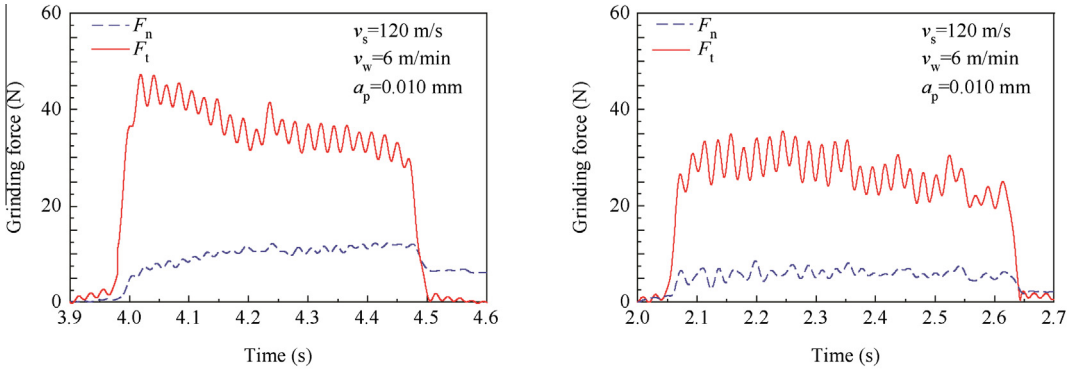

Fig. 4 Grinding forces signal.

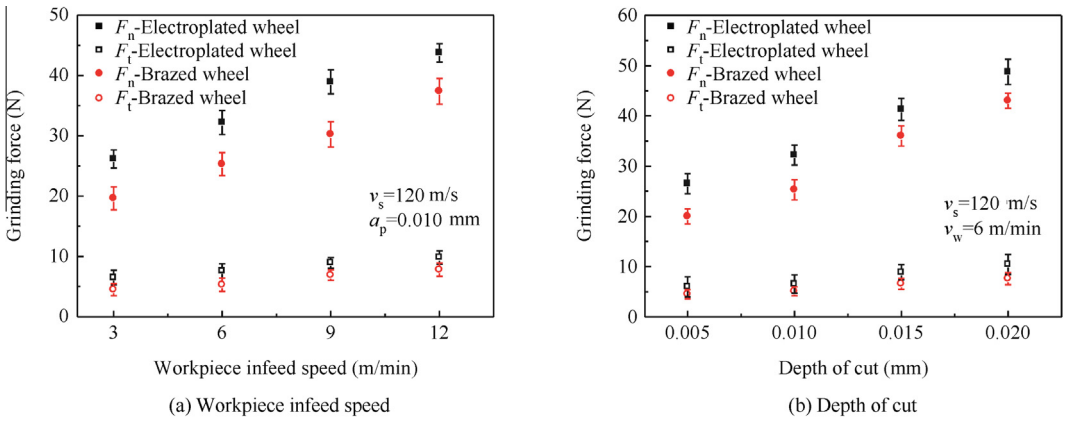

(a) Workpiece infeed speed (b) Depth of cut

Fig. 5 Effects of grinding parameters on grinding forces.

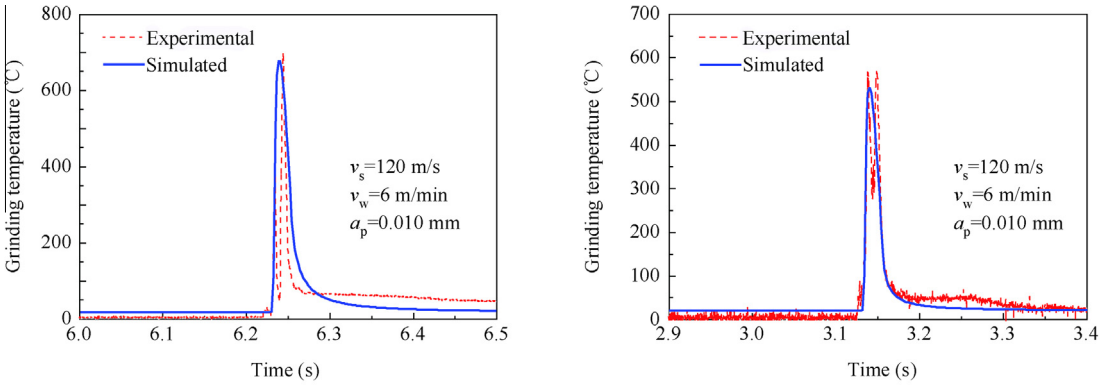

(a) Electroplated CBN wheel (b) Brazed CBN wheel

Fig. 6 Typical grinding temperature curves.

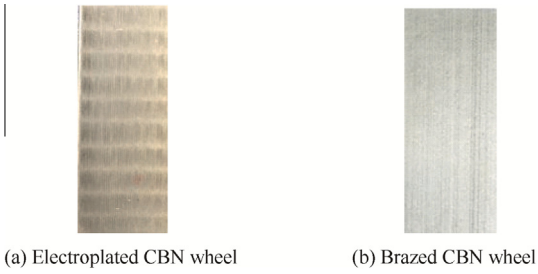

(a) Electroplated CBN wheel (b) Brazed CBN wheel

Fig. 7 PTMCs surface produced in high-speed grinding.

Fig. 10 displays the temperature distribution along a vertical direction from the ground surface to the workpiece interior part within the tool-workpiece contact zone. The variation of the temperature gradient along the grinding depth direction (i.e., a depth of 200 μm beneath the ground surface) could be observed. The grinding temperature in the tool-workpiece contact zone drops from the maximum temperature (i.e., 682 °C) on the surface to the lower temperature (i.e., 190 °C) at the depth of 250 μm when the electroplated CBN wheel is applied (Fig. 10(a)); meanwhile, the corresponding grinding temperature drops from 530 °C on the surface to 192 °C at the depth of 200 μm using the brazed wheel (Fig. 10(b)).

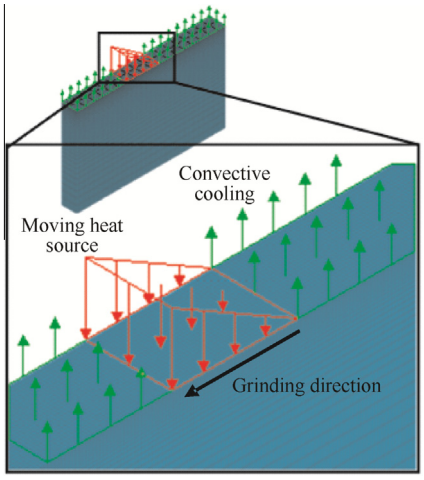

Fig. 8 Finite element model based on moving triangular heat source and convective cooling.

Fig. 11 displays the measured and simulated grinding temperature as functions of workpiece infeed speed and depth of cut. All the simulated temperature using the triangle heat source model shows a good agreement with those measured by the semi-artificial thermocouple method in the current

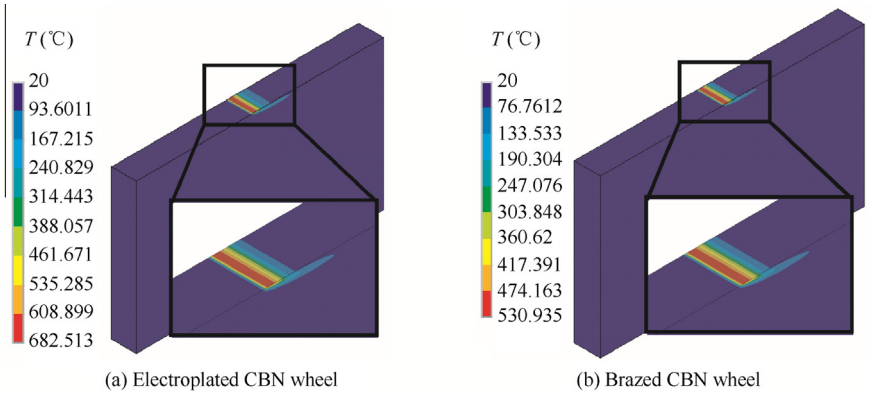

(a) Electroplated CBN wheel (b) Brazed CBN wheel

Fig. 9 Simulated grinding temperature distribution.

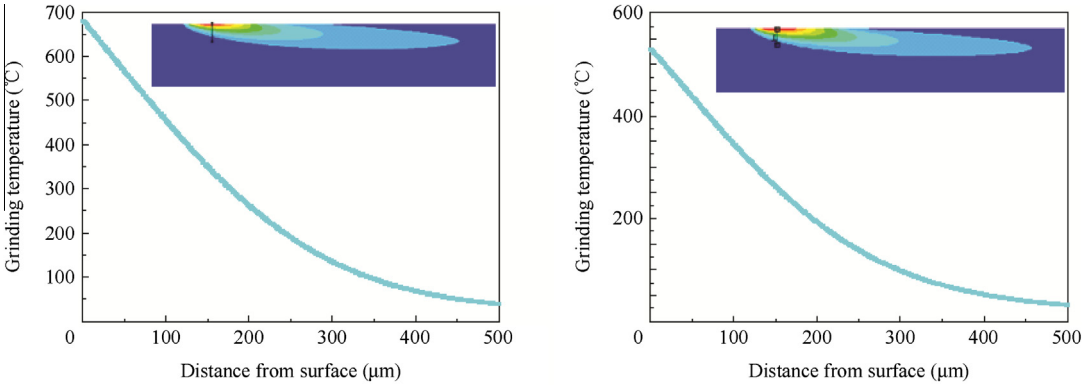

(a) Electroplated CBN wheel (b) Brazed CBN wheel

Fig. 10 Temperature distribution beneath workpiece surface along vertical direction.

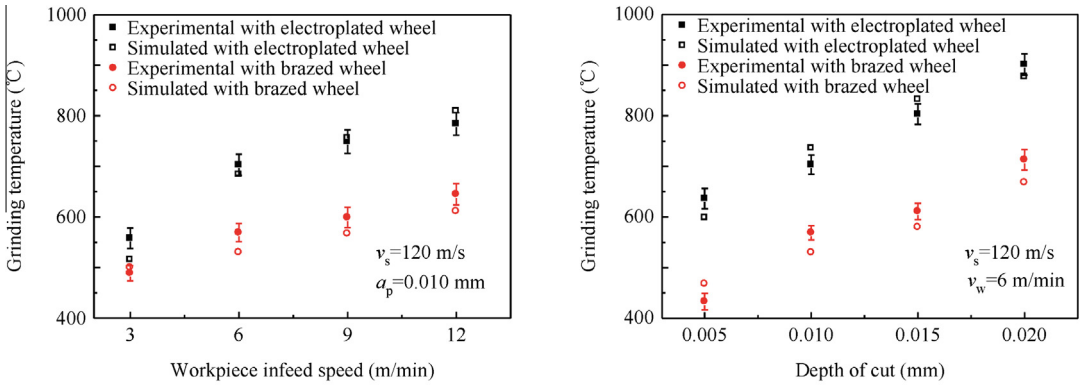

(a) Workpiece infeed speed (b) Depth of cut

Fig. 11 Effects of grinding parameters on grinding temperature.

high-speed grinding experiments. In general, the grinding temperature significantly increases with increasing of the workpiece infeed speed and depth of cut. Seen from Fig. 11 (a), when the depth of cut is 0.010 mm, and the workpiece infeed speed increases from 3 m/min to 12 m/min, the grinding temperature increases from 558 °C to 784 °C (by 40%) with the electroplated CBN wheel and from 489 °C to 645 °C (by 32%) with the brazed CBN one, respectively. When the depth of cut increases from 0.005 mm to 0.020 mm, and the workpiece infeed speed is fixed at 6 m/min, the grinding temperature rises rapidly from 636 °C to 901 °C (by 42%) with the electroplated wheel (Fig. 11(b)). For the single-layer brazed CBN wheel, the grinding temperature rises from 433 °C to 713 °C (by 65%). The reason for the above-mentioned variation phenomenon is that higher workpiece infeed speed or larger depth of cut always results in larger tangential force

(Fig. 5). As a consequence, more heat flux enters the grinding zone, which produces higher grinding temperature within the workpiece to a certain extent.

According to Fig. 11, it is also known that the grinding temperature obtained with the brazed CBN wheel is always lower than that with the electroplated wheel under the identical grinding parameters. Specifically, when larger workpiece infeed speed or higher depth of cut is utilized, the grinding temperature difference between the two CBN wheels is more significant, which is attributed to the different cooling conditions in the tool-workpiece contact zone formed with different CBN wheels in grinding.[29–31] Klocke and Baus have ever reported that the effective flow of coolants was proportional to the low grinding temperature.[32] In the current investigation, the difference of detailed cooling conditions formed with the electroplated CBN wheel and brazed counterpart is schematically demonstrated in Fig. 12. According to the Refs. 33 and 34, as for the electroplated CBN wheel, the grain protrusion is merely about 20%–30% of the whole grain particles; however, it could reach approximately 50%–70% of the whole grain particle for the brazed wheel. Here the grain protrusion refers to the particular part which is exposed beyond the connecting layer of the grinding wheel. Under such condition, when the electroplated CBN wheel is applied, the coolants could not make good effects due to the small space in the tool-workpiece contact zone during high-speed grinding. However, as for the brazed CBN wheel, the abundant storage space for coolants is provided owing to high grain protrusion, which ensures enough flow of the coolants and therefore excellent cooling effects are produced in high-speed grinding. For this reason, lower grinding temperature of PTMCs is always obtained with the single-layer brazed CBN wheel compared with the electroplated wheel. Quantitative analysis of the cooling effects in the tool-workpiece contact zone with the different single-layer CBN wheels will be an important topic in the further investigation.

Furthermore, because the burnout phenomenon of the PTMCs surface would take place once the grinding temperature exceeds 700 °C in the current experiments, the maximum materials removal rate could merely arrive at 1 $mm^3/(mm{\cdot}s)$ using the single-layer electroplated CBN wheel. Here the materials removal rate is the product of workpiece infeed speed and depth of cut. However, when the brazed CBN wheel is applied, even though the MRR has reached 2 $mm^3/(mm{\cdot}s)$, the highest grinding temperature is still below 700 °C (Fig. 11). That is to say, the maximum materials removal rate in high-speed grinding of PTMCs with the brazed CBN wheel is much larger than that with the electroplated wheel.

3.3. Grinding-induced surface features of PTMCs

The typical morphology of the ground PTMCs surface is shown in Fig. 13. Here two sets of grinding parameters are chosen: (i) the workpiece infeed speed of 6 m/min and the depth of cut of 0.005 mm; (ii) the worpiece infeed speed of 12 m/min and the depth of cut of 0.010 mm. The grinding-induced surface features, which are indicated by the number arrows from 1 to 6 in Fig. 13, include the grinding traces, fractured zone, voids, microcracks, debris adherence and smooth zone. Obviously, the voids and microcracks are always the dominant surface defects.

On one hand, in the high-speed grinding process of PTMCs, the voids are produced due to the fracture and pull-out of the TiC reinforcing particles under the grinding forces (Fig. 14). Meanwhile, it is found from Fig. 13 that the void size distinctly increases with increasing of the workpiece infeed speed and depth of cut for the two types of CBN wheels. The reason is that the undeformed chip thickness increases with increasing of workpiece infeed speed and depth of cut.[19,35] In other words, the effective CBN grains taking part in the grinding practice increase, and thereby the grinding force increases, which results in a great increasing of the void size in high-speed grinding.

On the other hand, the grinding-induced microcracks are observed in the current investigation (Fig. 15), which are obtained at the workpiece infeed speed of 6 m/min and depth of cut of 0.010 mm. Microcracks are produced due to the fracture behavior of the Ti–6Al–4V matrix materials under too large mechanical-thermal loads in grinding. For example, as displayed in Fig.6, in the current high-speed grinding process, the surface temperature in the tool-workpiece contact zone rises at a rate of 2.85×10^4 °C/s (from 20 °C to 703 °C within 0.024 s) and drops down to the lower temperature at 5.48×10^4 °C/s (from 703 °C to approximately 100 °C within 0.011 s) when the electroplated CBN wheel is utilized, while the temperature rises abruptly at 2.50×10^4 °C/s (from 20 °C to 569 °C within 0.022 s) and falls at 3.91×10^4 °C/s (from 569 °C to approximately 100 °C within 0.012 s) using the brazed CBN wheel. High grinding temperature and abrupt temperature variation could result in large residual tensile stresses within the surface/subsurface layer of the ground PTMCs specimens,[36–40] which have a key influence on the formation of grinding-induced microcracks.

3.4. Statistical analysis of grinding-induced surface defects of PTMCs

It is worth noting that, the voids and microcracks, as the major grinding-induced surface defects, have vital negative impacts on the ground surface quality. Therefore, the quantitatively statistical analysis of voids and microcracks is performed in the current investigation. The analysis procedure is as follows: firstly, ten grinding micro-regions with the same size are chosen randomly for each grinding parameter. For example, Fig. 16(a) shows one typical region ground with the

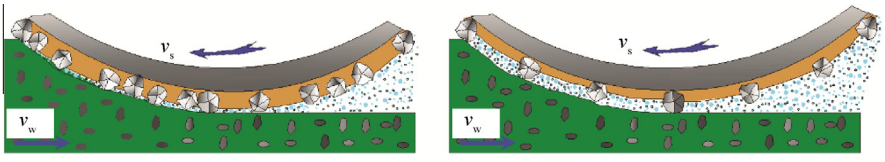

(a) Electroplated CBN wheel (b) Brazed CBN wheel

Fig. 12 Comparison of detailed cooling conditions within tool-workpiece contact zone.

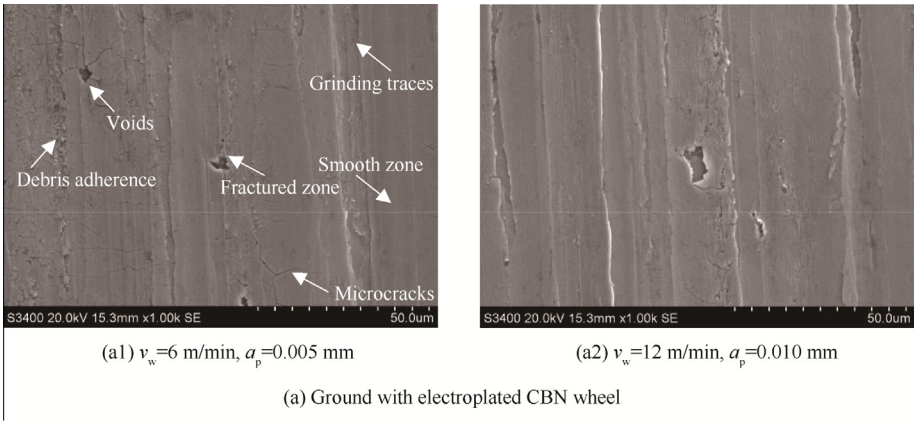

(a1) v_w=6 m/min, a_p=0.005 mm (a2) v_w=12 m/min, a_p=0.010 mm

(a) Ground with electroplated CBN wheel

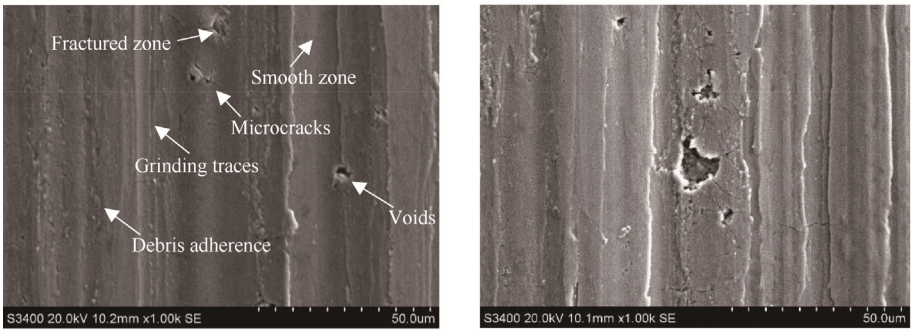

(b1) v_w=6 m/min, a_p=0.005 mm (b2) v_w=12 m/min, a_p=0.010 mm

(b) Ground with brazed CBN wheel

Fig. 13 Morphology of PTMCs surface produced in high-speed grinding.

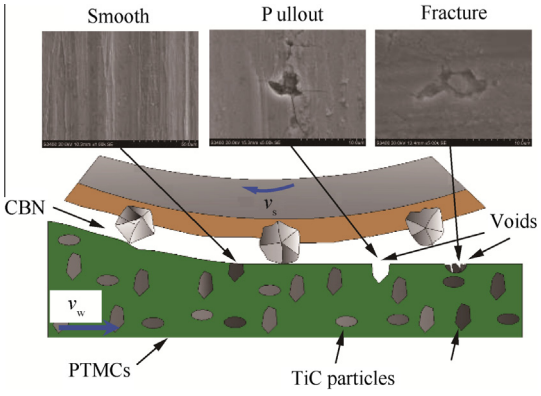

Fig. 14 Schematic of PTMCs surface features produced in high-speed grinding.

electroplated CBN wheel at the following grinding parameters: workpiece infeed speed of 6 m/min and depth of cut of 0.005 mm; Fig. 16(b) shows the region for another set of grinding parameters: workpiece infeed speed of 6 m/min and depth of cut of 0.010 mm; Fig. 16(c) is for workpiece infeed speed of 12 m/min and depth of cut of 0.010 mm. Secondly, the grinding-induced surface defects including the voids and microcracks are statistically analyzed. The voids (e.g., the area of the red rectangular region in Fig. 16) is calculated based on the single void area (e.g., <5 μm^2, 5–10 μm^2, >10 μm^2), while the microcracks (e.g., the yellow line in Fig. 16) are calculated according to single microcrack length (e.g., <6 μm, 6–9 μm, >9 μm). In particular, the above-mentioned critical values of the single void area and single microcrack length are determined according to the primary void area and microcrack length on the actual ground surface of PTMCs. Finally, the arithmetic average values obtained from the ten regions are applied as the final results under the corresponding grinding parameters (Fig. 17).

According to Fig. 17(a), the quantities of voids with an area of below 5 μm^2 are 89–105/mm^2 on the surface ground with the electroplated CBN wheel and 75–92/mm^2 with the brazed CBN wheel. However, for the voids with a larger area, especially for >10 μm^2, the voids quantities are 13–84/mm^2 using the electroplated CBN wheel and 8–70/mm^2 using the brazed wheel. The voids quantities obtained with the electroplated CBN wheel under the above-mentioned three grinding parameters are always larger than those with the brazed CBN wheel. The reason could be that the higher grinding force is produced using the single-layer electroplated CBN wheel (Fig. 5), and more reinforcing particles are therefore fractured or pulled out. Moreover, the voids quantities significantly increase with the increasing of grinding parameters from low to high level. For example, when the electroplated CBN wheel is utilized, the voids quantity with a larger area is merely 13 /mm^2 at the workpiece infeed speed of 6 m/min and the depth of cut of 0.005 mm, while it reaches 28/mm^2 at the workpiece infeed speed of 6 m/min and the depth of cut of 0.010 mm, and further rises to 84/mm^2 at the workpiece infeed speed of 12 m/min and the depth of cut of 0.010 mm. The reason for

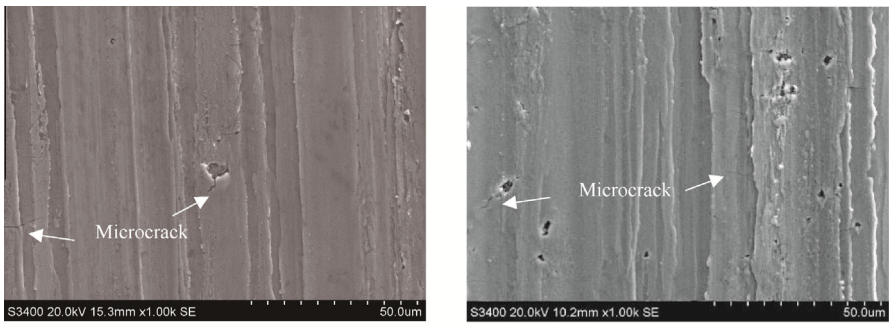

(a) Electroplated CBN wheel (b) Brazed CBN wheel

Fig. 15 Morphology of grinding-induced microcracks.

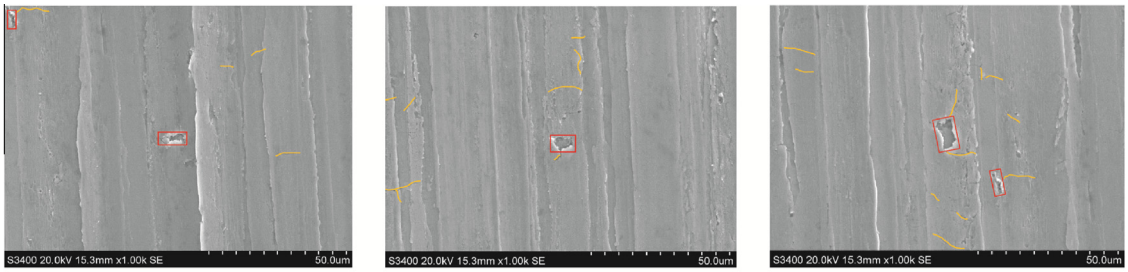

(a) v_w=6 m/min, a_p=0.005 mm (b) v_w=6 m/min, a_p=0.010 mm (c) v_w=12 m/min, a_p=0.010 mm

Fig. 16 Typical surface morphology obtained with single-layer electroplated CBN wheel under different high-speed grinding parameters.

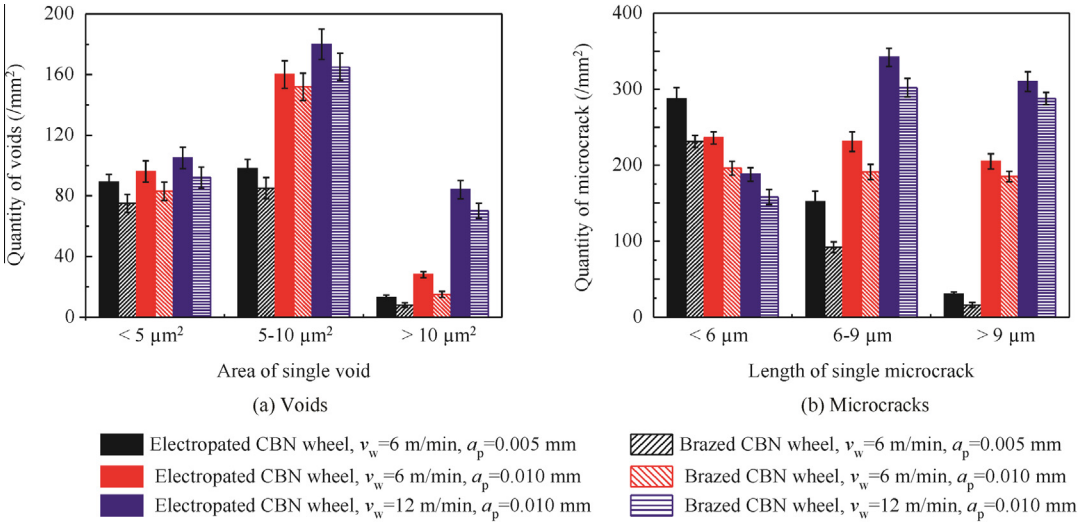

Fig. 17 Statistical analysis of different surface defects produced in high-speed grinding.

this phenomenon is also that the reinforcing particles fracture and pullout behavior becomes more serious under larger mechanical loads at larger grinding parameters.

As for the grinding-induced microcracks, the average quantities of microcracks with three different length scales increase with the increasing of the workpiece infeed speed and depth of cut (Fig. 17(b)). At the same time, it is also obvious that the quantities of the microcracks on the surface ground with the single-layer electroplated CBN wheel is always higher than those with the brazed CBN wheel under the identical grinding parameters. For example, when the workpiece infeed speed is 6 m/min and the depth of cut is 0.005 mm, the microcracks length is concentrated on <6 μm. At this time, the average quantities of the surface microcracks with a length of below 6 μm are 234/mm^2 with the brazed wheel and 287/mm^2 with the electroplated wheel. Furthermore, when the workpiece infeed speed increases to 12 m/min and the depth of cut increases to 0.010 mm, the concentration scale of microcrack length also gradually increases to 6–9 μm or beyond 9 μm. As for the surface ground with the brazed wheel, the average quantities are 302/mm^2 for the microcracks with a length of 6–9 μm and 288/mm^2 for the microcracks with a length beyond

9 μm. However, as for the electroplated wheel, they increase to 342 /mm^2 for the microcracks with a length of 6–9 μm and 310/mm^2 for the microcracks with a length beyond 9 μm. That is to say, less surface defects could be obtained when the brazed CBN super-abrasive wheel is utilized to grind PTMCs. In particular, the effects of the average quantities of grinding-induced voids and microcracks on the fatigue strength of the machined PTMCs components will be investigated in the further work.

4. Conclusions

High-speed grinding of PTMCs was carried out with the single-layer electroplated CBN wheel and single-layer brazed CBN wheel, respectively. The comparative grinding performance was investigated in terms of grinding force, grinding temperature and grinding-induced surface features and defects. The main conclusions are summarized as follows:

(1) Grinding forces and temperature obtained with the single-layer brazed CBN wheel are always lower than those with the electroplated CBN wheel. The burnout phenomenon takes place on the ground surface when the materials removal rate reaches 1 mm^3/(mm·s) with the electroplated CBN wheel; on the contrary, good surface is always obtained with the brazed wheel even though the materials removal rate exceeds 2 mm^3/(mm·s).
(2) The voids and microcracks are the dominant grinding-induced surface defects of PTMCs. However, according to the statistical analysis results of the voids and microcracks, less surface defects could be produced with the brazed CBN wheel.
(3) In general, compared with the single-layer electroplated CBN wheel, the single-layer brazed CBN wheel has greater potential in high-speed grinding of PTMCs owing to smaller grinding force, lower grinding temperature and less grinding-induced surface defects.

Acknowledgements

The authors gratefully acknowledge the financial support for this work by the National Natural Science Foundation of China (No. 51235004 and No. 51375235), the Fundamental Research Funds for the Central Universities (No. NE2014103), and the Science and Technology Supporting Program of Jiangsu Province (No. BE2013109 and No. BY2014003-008).

References

1. Klocke F, Soo SL, Karpuschewski B, Webster JA, Novovic D, Elfizy A, et al. Abrasive machining of advanced aerospace alloys and composites. *CIRP Ann* 2015;**64**(2):581–604.
2. Choi BJ, Kim IY, Lee YZ, Kim YJ. Microstructure and friction/wear behavior of (TiB + TiC) particulate-reinforced titanium matrix composites. *Wear* 2014;**318**:68–77.
3. Tjong SC, Mai YW. Processing-structure-property aspects of particulate-and whisker-reinforced titanium matrix composites. *Compos Sci Technol* 2008;**68**(3):583–601.
4. Siva SV, Ganguly RI, Srinivasarao G, Sahoo KL. Machinability of aluminum metal matrix composite reinforced with in-situ ceramic composite developed from mines waste colliery shale. *Mater Manuf Processes* 2013;**28**(10):1082–9.
5. Wang T, Xie L, Wang X, Ding Z. PCD tool performance in high-speed milling of high volume fraction SiCp/Al composites. *Int J Adv Manuf Technol* 2015;**78**(9–12):1445–53.
6. Huang S, Yu X, Wang F, Xu L. A study on chip shape and chip-forming mechanism in grinding of high volume fraction SiC particle reinforced Al-matrix composites. *Int J Adv Manuf Technol* 2015;**80**:1927–32.
7. Bejjani R, Shi B, Attia H, Balazinski M. Laser assisted turning of titanium metal matrix composite. *CIRP Ann* 2011;**60**(1):61–4.
8. Aramesh M, Shaban Y, Balazinski M, Attiac H, Kishawyd HA, Yacoutb S. Survival life analysis of the cutting tools during turning titanium metal matrix momposites (Ti-MMCs). *Proc CIRP* 2014;**14**:605–9.
9. Blau PJ, Jolly BC. Relationships between abrasive wear, hardness, and grinding characteristics of titanium-based metal-matrix composites. *J Mater Eng Perform* 2009;**18**(4):424–32.
10. Hood R, Cooper P, Aspinwall DK, Soo SL, Lee DS. Creep feed grinding of γ-TiAl using single layer electroplated diamond superabrasive wheels. *CIRP J Manuf Sci Technol* 2015;**11**:36–44.
11. Marschalkowski K, Biermann D, Weinert K. On the characteristics of high-performance internal peel grinding using electroplated CBN wheels. *Mach Sci Technol* 2012;**16**(4):580–600.
12. Aspinwall DK, Soo SL, Curtis DT, Mantle AL. Profiled superabrasive grinding wheels for the machining of a nickel based superalloy. *CIRP Ann* 2007;**56**(1):335–8.
13. Teicher U, Kunanz K, Ghosh A, Chattopadhyay AB. Performance of diamond and CBN single-layered grinding wheels in grinding titanium. *Mater Manuf Processes* 2008;**23**(3–4):224–7.
14. Ding WF, Xu JH, Chen ZZ, Su HH, Fu YC. Grindability and surface integrity of cast nickel-based superalloy in creep feed grinding with brazed CBN abrasive wheels. *Chin J Aeronaut* 2010;**23**(4):501–10.
15. Li BZ, Ni JM, Yang JG, Liang SY. Study on high-speed grinding mechanisms for quality and process efficiency. *Int J Adv Manuf Technol* 2014;**70**:813–9.
16. Yin L, Huang H, Ramesh K, Huang T. High speed versus conventional grinding in high removal rate machining of alumina and alumina-titania. *Int J Mach Tools Manuf* 2005;**45**(7–8):897–907.
17. Mao C, Zhang J, Huang Y, Zou HF, Huang XM, Zhou ZX. Investigation on the effect of nanofluid parameters on MQL grinding. *Mater Manuf Processes* 2013;**28**(4):436–42.
18. Huang H. Machining characteristics and surface integrity of yttria stabilized tetragonal zirconia in high speed deep grinding. *Mater Sci Eng A* 2003;**345**:155–63.
19. Tian L, Fu YC, Xu JH, Li HY, Ding WF. The influence of speed on material removal mechanism in high speed grinding with single grit. *Int J Mach Tools Manuf* 2015;**89**:192–201.
20. Ding WF, Xu JH, Shen M, Fu YC, Xiao B, Su HH, Xu HJ. Development and performance of monolayer brazed CBN grinding tools. *Int J Adv Manuf Technol* 2007;**34**:491–5.
21. Sun Y, Sun J, Li J, Xiong Q. An experimental investigation of the influence of cutting parameters on cutting temperature in milling Ti6Al4V by applying semi-artificial thermocouple. *Int J Adv Manuf Technol* 2014;**70**(5–8):765–73.
22. Zhang DK, Li CH, Jia DZ, Zhang YB, Zhang XW. Specific grinding energy and surface roughness of nanoparticle jet minimum quantity lubrication in grinding. *Chin J Aeronaut* 2015;**28**(2):570–81.
23. Zhang YB, Li CH, Jia DZ, Zhang DK, Zhang XW. Experimental evaluation of the lubrication performance of MoS2/CNT nanofluid for minimal quantity lubrication in Ni-based alloy grinding. *Int J Mach Tools Manuf* 2015;**99**:19–33.

24. Malkin S, Guo C. Thermal analysis of grinding. *CIRP Ann* 2007;**56**(2):760–82.
25. Li BK, Li CH, Zhang YB, Wang YG, Jia DZ, Yang M. Grinding temperature and energy ratio coefficient in MQL grinding of high-temperature nickel-base alloy by using different vegetable oils as base oil. *Chin J Aeronaut* 2016;**29**(4):1084–95.
26. Zhang YB, Li CH, Jia DZ, Zhang DK, Zhang XW. Lubricating property theoretical analysis and experimental evaluation on nano particle jet MQL grinding with vegetable oil as base oil. *J Cleaner Prod* 2015;**87**:930–40.
27. Jin T, Stephenson DJ, Rowe WB. Estimation of the convection heat transfer coefficient of coolant within the grinding zone. *Proc Inst Mech Eng Part B* 2004;**217**:397–407.
28. Rowe WB. Thermal analysis of high efficiency deep grinding. *Int J Mach Tools Manuf* 2001;**41**(1):1–19.
29. Davis TD, DiCorleto J, Sheldon D, Vecchiarelli J, Erkey C. A route to highly porous grinding wheels by selective extraction of pore inducers with dense carbon dioxide. *J Supercrit Fluids* 2004;**30**(3):349–58.
30. Shi CF, Li X, Chen ZT. Design and experimental study of a micro-groove grinding wheel with spray cooling effect. *Chin J Aeronaut* 2014;**27**(2):407–12.
31. Li X, Chen ZT, Chen WY. Suppression of surface burn in grinding of titanium alloy TC4 using a self-inhaling internal cooling wheel. *Chin J Aeronaut* 2011;**24**(1):96–101.
32. Klocke F, Baus A, Beck T. Coolant induced forces in CBN high speed grinding with shoe nozzles. *CIRP Ann* 2000;**49**(1):241–4.
33. Shi Z, Malkin S. Wear of electroplated CBN grinding wheels. *ASME J Manuf Sci Eng* 2006;**128**(1):110–8.
34. Ding WF, Xu JH, Chen ZZ, Su H, Fu YC. Wear behavior and mechanism of single-layer brazed CBN abrasive wheels during creep-feed grinding cast nickel-based superalloy. *Int J Adv Manuf Technol* 2010;**51**(5–8):541–50.
35. Hecker RL, Liang SY, Wu XJ, Xia P, Jin DGW. Grinding force and power modeling based on chip thickness analysis. *Int J Adv Manuf Technol* 2007;**33**(5–6):449–59.
36. Bell A, Jin T, Stephenson DJ. Burn threshold prediction for high efficiency deep grinding. *Int J Mach Tools Manuf* 2011;**51**(6):433–8.
37. Fergania O, Shaoa Y, Lazoglu I, Liang SY. Temperature effects on grinding residual stress. *Proc CIRP* 2014;**14**:2–6.
38. Chen X, Rowe WB, McCormack DF. Analysis of the transitional temperature for tensile residual stress in grinding. *J Mater Process Technol* 2000;**107**:216–21.
39. Xu XP, Yu YQ, Xu HJ. Effect of grinding temperatures on the surface integrity of a nickel-based superalloy. *J Mater Process Technol* 2002;**129**(1–3):359–63.
40. Yao CF, Jin QC, Huang XC, Wu DX, Ren JX, Zhang DH. Research on surface integrity of grinding Inconel 718. *Int J Adv Manuf Technol* 2013;**65**(5–8):1019–30.

Li Zheng is a Ph.D. student in the College of Mechanical and Electrical Engineering at Nanjing University of Aeronautics and Astronautics in China. His research interest is grinding technology of difficult-to-cut materials.

Ding Wenfeng is a professor and Ph.D. supervisor in the College of Mechanical and Electrical Engineering at Nanjing University of Aeronautics and Astronautics in China. His research interests include grinding technology of difficult-to-cut materials and fabrication technology of brazed CBN superabrasive tools.